

Anionic Regulated NiFe (Oxy)Sulfide Electrocatalysts for Water Oxidation

Bo-Quan Li, Shu-Yuan Zhang, Cheng Tang, Xiaoyang Cui, and Qiang Zhang*

The construction of active sites with intrinsic oxygen evolution reaction (OER) is of great significance to overcome the limited efficiency of abundant sustainable energy devices such as fuel cells, rechargeable metal–air batteries, and in water splitting. Anionic regulation of electrocatalysts by modulating the electronic structure of active sites significantly promotes OER performance. To prove the concept, NiFeS electrocatalysts are fabricated with gradual variation of atomic ratio of S:O. With the rise of S content, the overpotential for water oxidation exhibits a volcano plot under anionic regulation. The optimized NiFeS-2 electrocatalyst under anionic regulation possesses the lowest OER overpotential of 286 mV at 10 mA cm⁻² and the fastest kinetics being 56.3 mV dec⁻¹ to date. The anionic regulation methodology not only serves as an effective strategy to construct superb OER electrocatalysts, but also enlightens a new point of view for the in-depth understanding of electrocatalysis at the electronic and atomic level.

The exhaustion of traditional fossil fuels and growing demand of energy encourage us to develop sustainable and clean energy systems, such as fuel cells, rechargeable metal–air batteries, and water splitting devices.^[1] Oxygen evolution reaction (OER) constitutes the core process but severely limits the efficiency of the above energy devices due to its sluggish kinetics.^[2,3] Many OER electrocatalysts have been proposed,^[4] among which ionic compounds are widely investigated and exhibit outstanding reactivity.^[5] Yet, new insights into OER electrocatalysis are still in urgent request for rational design of superb OER electrocatalysts.

The construction of active sites with extraordinary intrinsic water oxidation reactivity is of great significance toward OER electrocatalysis. A pivotal issue of rational

electrocatalyst design is to optimize the electronic structure of the active sites to facilitate water oxidation.^[6] OER is a typical surface reaction consisting of reactant adsorption, electron transfer, and product desorption.^[3,7] Appropriate electronic structure of active sites is favorable for the above processes and therefore the electrocatalyst exhibits superb OER reactivity. Therefore, effective regulation of the electronic structure of the active sites is the key to superb OER performance.

The electronic structure is usually regulated by coordination of multiple elements in inorganic compounds. Doping, etching, and substitution of ions are widely accepted to modulate the electronic structure and therefore enhance the OER performance.^[8] Cationic regulation has been a mature method by the substitution of the cations of the electrocatalysts. For instance, Sr²⁺ was doped into PrBa_{1-x}Sr_xCo₂O_{5+δ} perovskite to regulate the concentration of surface Co⁴⁺ for OER promotion.^[9] The exploration of Mn doping toward NiFe hydroxides,^[10] the electronic structure regulated by Co incorporation,^[11] and Fe-doped nickel sulfides as efficient OER electrocatalysts^[12] were also highly concerned.

Anionic regulation is another promising route to tune the electronic structure of an inorganic materials.^[13] Specifically, anions serve as electron donors and militate the cations by electron interactions. The nature of the anions determines the properties of the interaction and the reactivity of the active

B.-Q. Li, S.-Y. Zhang, C. Tang, Dr. X. Y. Cui,
Prof. Q. Zhang
Beijing Key Laboratory of Green Chemical Reaction
Engineering and Technology
Department of Chemical Engineering
Tsinghua University
Beijing 100084, China
E-mail: zhang-qiang@mails.tsinghua.edu.cn



 The ORCID identification number(s) for the author(s) of this article can be found under <http://dx.doi.org/10.1002/smll.201700610>.

DOI: 10.1002/smll.201700610

sites. Particularly, the polarization of the anions is crucial to the overall electronic structure of the active sites because it regulates the covalency and the ionicity of the interactions between cations and anions.^[14] Herein, the anionic regulation strategy is proposed to tune the electronic structure of the OER active sites by modulating anions in typical NiFe (oxy) sulfide electrocatalysts.

The concept of anionic regulation is illustrated in **Figure 1**. Metal cations constitute the actual active sites of OER reaction, while the adjacent anions regulate the electronic structure of the active sites. Nonpolarized anions appear as dominant ionicity and the electron interaction is weak. The cations provide strong positive electric field, which is favorable for the adsorption of negative hydroxyl but adverse to oxygen desorption, as shown in Figure 1a. In contrast, polarized anions afford electrons into the empty orbits of the cations to promote the covalency of the interaction. However, when the anions adjacent to the central cations are dominantly polarized, the reactants cannot feel enough positive electric field and therefore the adsorption of hydroxyl is deficient (Figure 1c). When a suitable polarization degree is attained (Figure 1b), the electronic structure of the active sites is optimized by coordination of the covalency and ionicity of the interaction between anions and cations. Such tunable electronic structure facilitates the adsorption, electron transfer, and desorption process simultaneously and the as-obtained electrocatalyst therefore exhibits superb OER performance.

To verify the concept of anionic regulation, the couple of oxygen and sulfur is selected as tunable anions, with NiFe serving as the cationic component regarded as superior active sites for OER in many cases.^[15] Oxygen anions are typical hard anions and usually nonpolarized, while sulfur anions are soft and tend to be polarized in sulfides. Moreover, oxygen and sulfur derive from the same VIA group of the periodic table which reduces the difficulty of anionic regulation.^[16] A series of S–O anionic regulated electrocatalysts were fabricated with similar morphology but gradually varied composition of the anions. The OER reactivity of the as-obtained electrocatalysts are therefore sufficiently regulated, exhibiting a volcano plot describing the overpotential at 10.0 mA cm⁻² depending on the atomic ratio of S:O. The

optimized electrocatalyst under anionic regulation demonstrates superb performance toward OER (286 mV at 10.0 mA cm⁻²) and water splitting (1.64 V at 10.0 mA cm⁻²), even better than the state-of-the-art IrO₂ electrocatalyst.

The apparent OER performance is otherwise limited by the amount of active sites exposed to reactants and electrons.^[16,17] In order to verify the anionic regulation strategy, such limitation should be eliminated to guarantee that the OER performance can sufficiently demonstrate the intrinsic reactivity of the anionic regulated electrocatalysts. Therefore, a pomegranate-like nanostructured electrocatalyst with nanosized active phases hybridized into a 3D conductive framework is selected to evaluate the intrinsic reactivity of the NiFe-based electrocatalysts.^[18] A novel spatially confined synthetic method is introduced (**Figure 2a**) in which 3D graphene framework (GF) with abundant 5–10 nm mesopores was applied to spatially confine the growth of active species (Figure 2b and Figure S1 (Supporting Information)).

NiFe layered double hydroxide (NiFeLDH) nanoparticles with a size range of 3–8 nm were then synthesized by in situ coprecipitation with GF, resulting in a pomegranate-like structure of NiFeLDH precursor (Figure 2c and Figure S2 (Supporting Information)). The X-ray diffraction (XRD) patterns (Figure S3, Supporting Information) demonstrate the hydroxide phase of the NiFeLDH precursor (PDF#38-0715). The Ni/Fe ratio of the NiFeLDH precursor is determined to be 2.85 and 3.05 by X-ray photoelectron spectroscopy (XPS) and energy disperse spectroscopy (EDS), respectively (Figure S4, Supporting Information). Such nanosized NiFeLDH precursor guarantees the anionic regulation of vulcanization and fully exposure of active sites toward reactants.

The anionic regulation of the electrocatalysts was realized by vulcanization of the NiFeLDH precursor using thioacetamide (TAA) as the vulcanization reagent.^[19] The resultant is named as NiFeS-*x*, where *x* marks the mass ratio of TAA:NiFeLDH. As illustrated in Figure 2d and Figure S5 (Supporting Information), NiFeS-2 exhibits a morphology of NiFeS nanoparticles with an average diameter of ≈20 nm hybridized with GF. Further high-resolution transmission electron microscope (TEM) image (Figure 2e) and XRD patterns (Figure 2f) identify that the phase of NiFeS-2 is (NiFe)₂S₂ (PDF#88-1701), with the observed lattice fringe being (1 0 0) and the corresponding interplanar spacing being 0.532 nm. The S and O content is calculated to be 18.7 and 13.0 at%, respectively, by XPS spectrum in Figure S6 (Supporting Information).

The nonvulcanized NiFeS-0 was synthesized without adding TAA agent. The morphology (Figure S7, Supporting Information) and the XRD pattern (Figure S8, Supporting Information) of NiFeS-0 electrocatalyst are similar to those of the NiFeLDH precursor, suggesting no obvious change with aspect of structure or constitution. The sulfur content of NiFeS-0 is less than 1.0 at%, which is similar to the analysis result for NiFeLDH (Figure S9, Supporting Information). NiFeS-0.5 is the

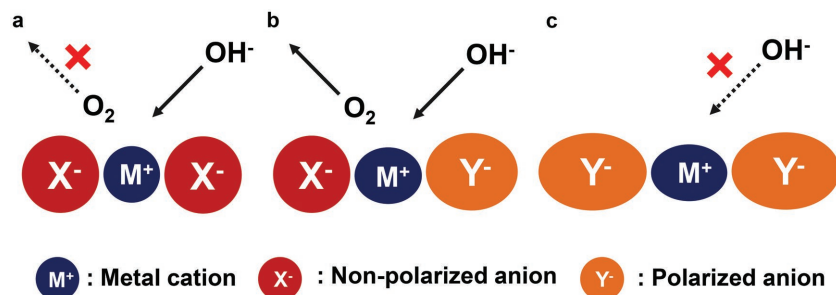


Figure 1. Schematic of anionic regulation by optimizing the electronic structure of active sites toward water oxidation. a) The cations provide strong positive electric field which is favorable for the adsorption of negative hydroxyl but adverse to oxygen desorption; b) The optimized electronic structure under anionic regulation facilitates the adsorption of reactants, electron transfer, and product desorption, therefore, promotes the OER electrocatalysis; c) When the anions adjacent to the central cations are dominantly polarized, the reactants cannot feel enough positive electric field and therefore the adsorption of hydroxyl is deficient.

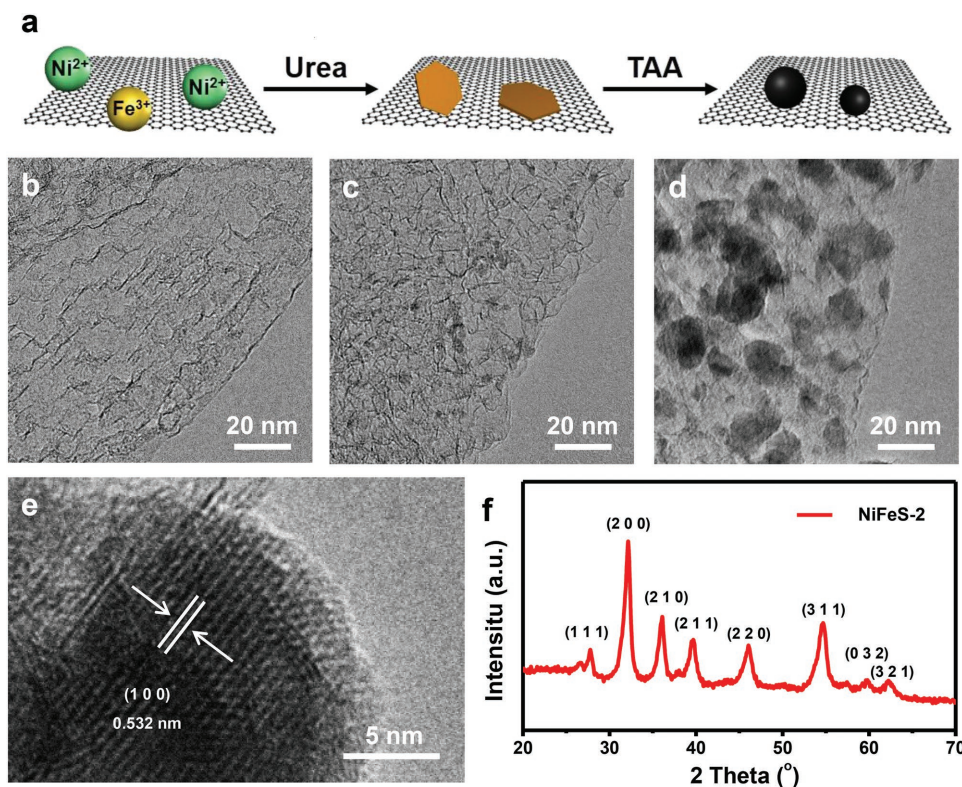


Figure 2. Structure characterization of anionic regulated electrocatalysts. a) Scheme of spatially confined synthesis of NiFeS electrocatalysts by coprecipitation and vulcanization. TEM images of b) GF, c) NiFeLDH, and d) NiFeS-2. e) High-resolution TEM image and f) XRD patterns of NiFeS-2 electrocatalyst.

slightly vulcanized sample, demonstrating the morphology of NiFeLDH being in process of transformation (Figure S10, Supporting Information). The sulfur content sharply increases to 7.0 at% (Figure S11, Supporting Information). The XRD pattern exhibits a mixture of hydroxides and sulfides (Figure S12, Supporting Information). As for the overvulcanized NiFeS-8 with extra TAA added, the NiFeS nanoparticles are larger than NiFeS-2 but still within the size of 50 nm (Figure S13, Supporting Information). A very high sulfur content of 39.5 at% is detected on NiFeS-8 electrocatalyst (Figure S14, Supporting Information), and $(\text{NiFe})\text{S}_2$ is identified to be the main phase of NiFeS-8, with partial FeNi_2S_4 (PDF#42-1449) observed (Figure S15, Supporting Information). The NiFeS-*x* electrocatalysts derived from NiFeLDH precursor share similar morphology with nanosized NiFeS particles hybridized with conductive GF, guaranteeing the fully exposure of active sites and sufficient conductivity toward OER electrocatalysis.

In order to identify the composition of anionic regulated NiFeS electrocatalysts, XPS and EDS were carried out to obtain the surface and bulk compositions. In **Figure 3a**, both XPS and EDS exhibit similar results of the atomic ratio of Ni:Fe being close to 3, demonstrating that the Ni:Fe atomic ratio of the NiFeS electrocatalysts is quite stable against vulcanization. However, the atomic ratio of S:O demonstrates obvious variation as expected. With the addition of TAA as vulcanization reagent, sulfur gradually substitutes the original oxygen to form anionic regulated electrocatalysts. The atomic ratio of S:O rises from 0.025 (NiFeS-0) to 2.35 (NiFeS-8) as characterized by XPS. The EDS results are coincident with

XPS analysis, with the atomic ratio of S:O raising rapidly. No oxygen is detected in NiFeS-2 or NiFeS-8 by EDS analysis, indicating the efficient vulcanization. The element analysis confirms the successful fabrication of anionic regulated electrocatalysts, making ready for further OER performance characterization (Table S1, Supporting Information).

The OER performance was characterized using a three-electrode system in O_2 -saturated 0.10 M KOH electrolyte at room temperature. Figure 3b demonstrates the linear sweep voltammetry (LSV) profiles calibrated with 95% *iR*-compensation. The redox peaks around 1.44 V versus reversible hydrogen electrode (RHE) is ascribed to the $\text{Ni}^{2+}/\text{Ni}^{3+}$ redox process. The overpotential at 10.0 mA cm^{-2} is usually selected as the core parameter to evaluate the OER reactivity.^[7] As illustrated in Figure 3c, OER reactivity is effectively regulated by anionic substitution. The overpotential at 10.0 mA cm^{-2} decreases from 329 mV (NiFeS-0), 308 mV (NiFeS-0.5), to an optimized 286 mV (NiFeS-2) but increases to 364 mV for NiFeS-8, exhibiting a unique volcano plot under anionic regulation. Tafel plots were calculated using the LSV curves according to the Tafel equation $\eta = b \log(j/j_0)$, where η is the overpotential, j is the current density, j_0 is the exchange current density, and b is the Tafel slope. The Tafel plots in Figure S16 (Supporting Information) exhibit similar tendency over anionic regulation, with the NiFeS-2 electrocatalyst possessing the fastest kinetics being 56.3 mV dec^{-1} . By fitting the OER reactivity with anionic constitution, the anionic regulation strategy is proved to be very effective for water oxidation enhancement.

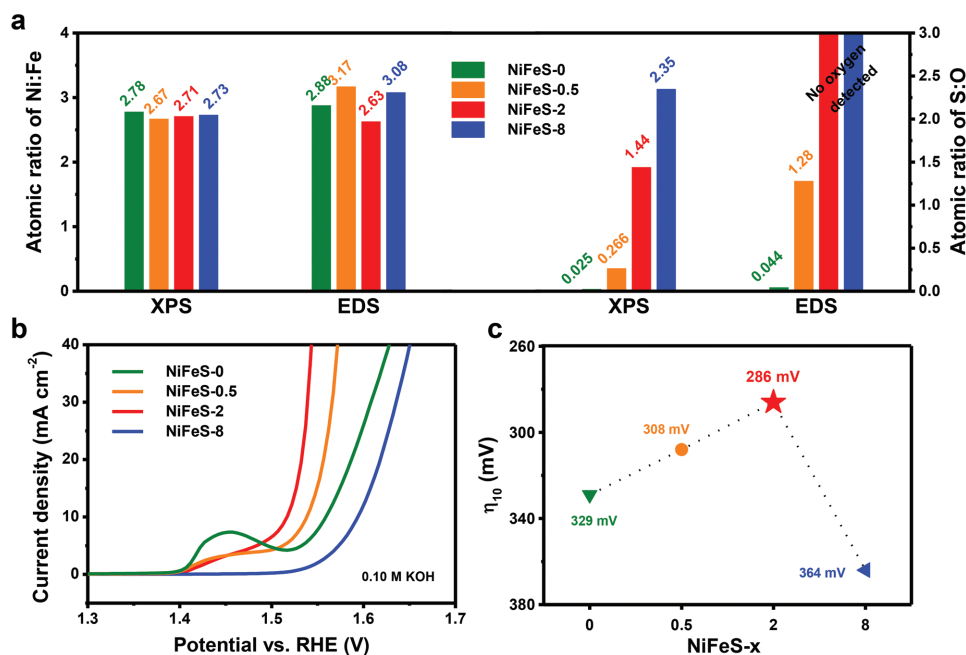


Figure 3. Elemental composition analysis of NiFeS-*x* electrocatalysts and corresponding OER reactivity. a) Atomic ratio of Ni:Fe and S:O of NiFeS-*x* electrocatalysts determined by XPS and EDS. b) 95% *iR*-compensated LSV profiles at a scan rate of 10.0 mV s⁻¹ in O₂-saturated 0.10 M KOH. c) Volcano plots of OER reactivity characterized by the overpotential at 10.0 mA cm⁻² against the vulcanization degree under anionic regulation.

To further probe the mechanism of the anionic regulation strategy, high-resolution XPS analysis was performed (**Figure 4**). With the substitution of sulfur, high-resolution S 2p XPS spectra exhibit an increased content of sulfur. The profiles shift to lower binding energy, which is typical for sulfides.^[20,21] The O 2p XPS spectra exhibit similar shifting to lower binding energy, which is induced by the polarization effect of sulfur component.^[21] Despite that the Fe 2p XPS spectra remain identical among the samples, the high-resolution XPS spectra of Ni 2p demonstrate obvious shifting to lower binding energy, suggesting lower oxidative state by receiving more electrons under anionic regulation. Sulfur anions are easily polarized and further share dispersive electrons with adjacent metal ions. The electron interaction promotes the covalency of the bonds between cations and anions. With more electrons achieved, the nickel cationic sites afford less positive electronic field, which is unambiguously proved by the Ni 2p XPS spectra. Notably, the nickel redox around 1.44 V versus RHE in Figure 3b decreases with the substitution of sulfur, which affords a side evidence of

nickel accepting electrons and becoming more difficult to be oxidized. In contrast, the oxygen anions serve as nonpolarized components and play the opposite role to regulate the interactions favorable to ionicity. By anionic regulation of oxygen and sulfur, the electronic structure of the active sites is significantly modulated. With the fine balance of covalency and ionicity and optimized electronic structure of active sites under anionic regulation, the NiFeS-2 electrocatalyst exhibits superb performance for OER.

In order to probe the practical performance of the anionic regulated electrocatalysts, more electrochemical tests were carried out. The optimized NiFeS-2 exhibits an ultralow overpotential at 10.0 mA cm⁻² toward OER (286 mV) and is 94 mV lower than the state-of-the-art IrO₂ (380 mV) (**Figure 5a**), which is among the best OER electrocatalysts till now (Table S2, Supporting Information). The Tafel slope is also significantly decreased from 108 mV dec⁻¹ for IrO₂ to 56.3 mV dec⁻¹ for NiFeS-2 (Figure 5a, inserted). The NiFeS-2 also delivers the largest electrochemical active surface area (ECSA) among all the NiFeS-*x* electrocatalysts (Figure S17, Supporting

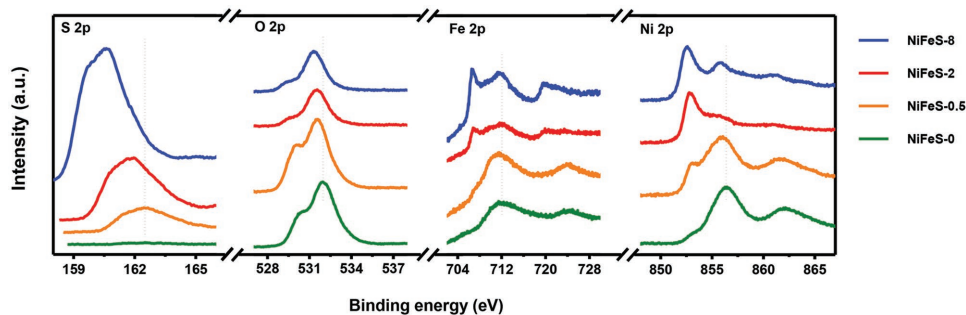


Figure 4. High-resolution S 2p, O 2p, Fe 2p, and Ni 2p XPS spectra of NiFeS-*x* electrocatalysts. The anionic regulated electrocatalysts exhibit the shifting to lower binding energy with aspects of S, O, and Ni spectra.

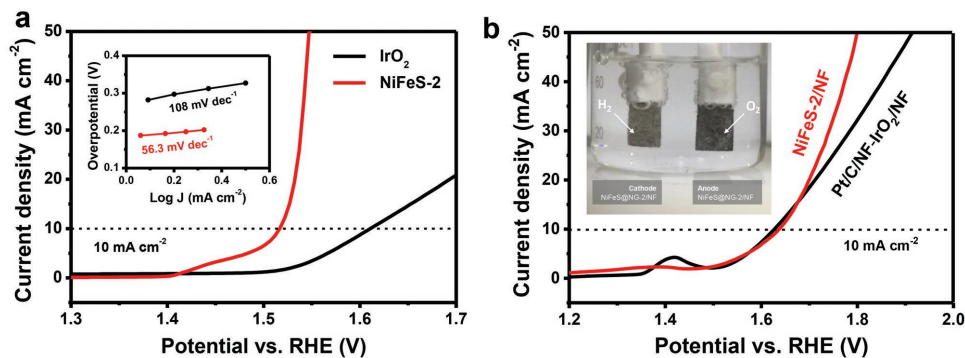


Figure 5. Electrochemical evaluation of the optimized NiFeS-2 electrocatalyst under anionic regulation. a) OER LSV profiles and inserted Tafel plots of NiFeS-2 and IrO₂ electrocatalysts in O₂-saturated 0.10 M KOH. b) LSV profiles and inserted picture of NiFeS-2 and Pt/C-IrO₂ electrocatalyst for overall water splitting in N₂-saturated 1.0 M KOH.

Information). In addition, NiFeS-*x* electrocatalysts exhibit superb conductivity evaluated by electrochemical impedance spectroscopy (EIS) in Figure S18 (Supporting Information), which is attributed to the hybridization with conductive graphene framework. The stability of NiFeS-2 against OER was tested by comparing the OER profiles before and after long-time durability tests at a constant potential required to reach an initial current density of 10.0 mA cm⁻². The overpotential at 10.0 mA cm⁻² increases 20 mV after 10 000 s and 48 mV after 20 000 s (Figure S19, Supporting Information), exhibiting excellent stability toward OER. The morphology of NiFeS-2 remains the same as the pristine electrocatalyst, confirming the robust structure and stability of the NiFeS-2 electrocatalyst (Figure S20, Supporting Information).

Hydrogen evolution reaction (HER) was characterized in N₂-saturated 1.0 M KOH electrolyte. The LSV curves in Figure S21 (Supporting Information) demonstrate that NiFeS-2 possesses the ability to catalyze HER but inferior to Pt/C. The overpotential at 10.0 mA cm⁻² is 281 mV comparable to other HER electrocatalysts (Table S3, Supporting Information).

The overall water splitting performance of NiFeS-2 was tested in N₂-saturated 1.0 M KOH using a two-electrode system (Figure 5b, inserted). NiFeS-2 was coated onto nickel foam (NF) with an areal loading of 0.25 mg cm⁻². Pt/C/NF and IrO₂/NF electrodes were fabricated using the same method for comparison. The potential required to reach 10.0 mA cm⁻² is 1.64 V, which is only 20 mV higher than the state-of-the-art Pt/C-IrO₂ electrocatalysts, exhibiting extraordinary water splitting reactivity considering the low areal loading of the working electrode (Table S4, Supporting Information). The LSV curves of water splitting on NF supported NiFeS-2 electrocatalyst demonstrate a tiny rise of overpotential at 10.0 mA cm⁻² after a 40 000 s durability test (Figure S22, Supporting Information), suggesting excellent stability in practical use. The optimized NiFeS-2 under anionic regulation possesses superb performance toward overall water splitting and is remarkably promising for further applications.

Considering the superior OER performance of the NiFeS electrocatalysts, it is necessary to inquire into the anionic regulation methodology at electronic and atomic level. The NiFe component serves as active sites toward water oxidation, whose intrinsic active 3d electrons can be transferred during

OER electrocatalysis. The property of the active 3d electrons is highly dependent on the electronic structure of the overall NiFe active sites, which can be significantly affected by adjacent anions. The anionic regulation methodology herein is to modulate the NiFe active sites using antagonistic oxygen and sulfur anions. The nonpolarized oxygen anions hold their electrons tightly, rendering high ionicity and intense positive electric field of cations, which is unfavorable for oxygen desorption. In contrast, the polarized sulfur anions tend to give their dispersive electrons to the empty orbits of NiFe sites and therefore promote the covalency of the interaction between cations and anions. When the antagonistic effect is balanced, the overall active domain affords optimized electronic structure and exhibits superior reactivity toward water oxidation. The anionic regulation methodology affords a fresh insight into ionic interactions and electrocatalyst design for OER, closely associating the microscopic electronic structure with the macroscopic electrocatalytic performance.

In summary, we propose the novel strategy of anionic regulation to modulate the electronic structure of active sites in NiFe (oxy)sulfides for promoting OER performance. The proof-of-concept NiFeS electrocatalysts were fabricated with gradual variation of atomic ratio of S:O. The polarized sulfur anions and the nonpolarized oxygen anions synergetically regulate the electronic structure of the active sites by electron interaction with the cations. Dispersive electrons of polarized anions are shared with adjacent cations and thus regulate the covalency and ionicity of the interactions between cations and anions. The optimized electrocatalyst under anionic regulation exhibits superb reactivity toward OER (286 mV at 10 mA cm⁻²) and is much better than the state-of-the-art IrO₂. The anionic regulation methodology not only serves as an effective strategy to construct superb OER electrocatalysts, but also enlightens a new point of view of in-depth understanding of electrocatalysis at electronic and atomic level.

Supporting Information

Supporting Information is available from the Wiley Online Library or from the author.

Acknowledgements

B.-L.L. and S.-Y.Z. contributed equally to this work. This work was supported by the National Key Research and Development Program (No. 2016YFA0202500), the Natural Scientific Foundation of China (No. 21422604), and the Tsinghua University Initiative Scientific Research Program. The authors thank Hao-Fan Wang, Chen-Yu Chen, and Zi-Jing Xia for helpful discussion.

Conflict of Interest

The authors declare no conflict of interest.

- [1] a) J. Suntivich, H. A. Gasteiger, N. Yabuuchi, H. Nakanishi, J. B. Goodenough, Y. Shao-Horn, *Nat. Chem.* **2011**, *3*, 546; b) S. Chu, Y. Cui, N. Liu, *Nat. Mater.* **2017**, *16*, 16; c) J. Zhang, Z. Zhao, Z. Xia, L. Dai, *Nat. Nanotechnol.* **2015**, *10*, 444; d) M. Kuang, G. F. Zheng, *Small* **2016**, *12*, 5656; e) W. W. Xu, Z. Y. Lu, P. B. Wan, Y. Kuang, X. M. Sun, *Small* **2016**, *12*, 2492; f) S. Chen, J. Duan, Y. Zheng, X. Chen, X. W. Du, M. Jaroniec, S.-Z. Qiao, *Energy Storage Mater.* **2015**, *1*, 17.
- [2] a) I. Katsounaros, S. Cherevko, A. R. Zeradjanin, K. J. J. Mayrhofer, *Angew. Chem., Int. Ed.* **2014**, *53*, 102; b) W. Zhang, W. Lai, R. Cao, *Chem. Rev.* **2017**, *117*, 3717.
- [3] Y. Jiao, Y. Zheng, M. Jaroniec, S. Z. Qiao, *Chem. Soc. Rev.* **2015**, *44*, 2060.
- [4] a) J. Zhang, T. Wang, D. Pohl, B. Rellinghaus, R. Dong, S. Liu, X. Zhuang, X. Feng, *Angew. Chem., Int. Ed.* **2016**, *55*, 6701; b) D.-W. Wang, D. Su, *Energy Environ. Sci.* **2014**, *7*, 576; c) X. Q. Zhang, X. B. Cheng, Q. Zhang, *J. Energy Chem.* **2016**, *25*, 967; d) W. Zhou, X.-J. Wu, X. Cao, X. Huang, C. Tan, J. Tian, H. Liu, J. Wang, H. Zhang, *Energy Environ. Sci.* **2013**, *6*, 2921; e) Z. Wang, Y. Lu, Y. Yan, T. Y. P. Larissa, X. Zhang, D. Wu, H. Zhang, Y. Yang, X. Wang, *Nano Energy* **2016**, *30*, 368; f) J. Suntivich, K. J. May, H. A. Gasteiger, J. B. Goodenough, Y. Shao-Horn, *Science* **2011**, *334*, 1383; g) C. Tang, H.-F. Wang, X. Chen, B.-Q. Li, T.-Z. Hou, B. Zhang, Q. Zhang, M.-M. Titirici, F. Wei, *Adv. Mater.* **2016**, *28*, 6845; h) Y. C. Pi, N. Zhang, S. J. Guo, J. Guo, X. Q. Huang, *Nano Lett.* **2016**, *16*, 4424; i) N. Y. Cheng, Q. Liu, A. M. Asiri, W. Xing, X. P. Sun, *J. Mater. Chem. A* **2015**, *3*, 23207; j) R. Li, Z. D. Wei, X. L. Gou, *ACS Catal.* **2015**, *5*, 4133; k) G. L. Tian, M. Q. Zhao, D. S. Yu, X. Y. Kong, J. Q. Huang, Q. Zhang, F. Wei, *Small* **2014**, *10*, 2251.
- [5] a) L. Han, X.-Y. Yu, X. W. Lou, *Adv. Mater.* **2016**, *28*, 4601; b) J. Ping, Y. Wang, Q. Lu, B. Chen, J. Chen, Y. Huang, Q. Ma, C. Tan, J. Yang, X. Cao, Z. Wang, J. Wu, Y. Ying, H. Zhang, *Adv. Mater.* **2016**, *28*, 7640; c) T. Y. Ma, J. L. Cao, M. Jaroniec, S. Z. Qiao, *Angew. Chem., Int. Ed.* **2016**, *55*, 1138; d) J. Wang, C. F. Tan, T. Zhu, G. W. Ho, *Angew. Chem., Int. Ed.* **2016**, *55*, 10326; e) Y. Zhang, B. Ouyang, J. Xu, G. Jia, S. Chen, R. S. Rawat, H. J. Fan, *Angew. Chem., Int. Ed.* **2016**, *55*, 8670; f) Y. Zhu, W. Zhou, Z.-G. Chen, Y. Chen, C. Su, M. O. Tade, Z. Shao, *Angew. Chem., Int. Ed.* **2015**, *54*, 3897; g) Z. Lu, W. Xu, W. Zhu, Q. Yang, X. Lei, J. Liu, Y. Li, X. Sun, X. Duan, *Chem. Commun.* **2014**, *50*, 6479; h) X.-Y. Yu, Y. Feng, B. Guan, X. W. Lou, U. Paik, *Energy Environ. Sci.* **2016**, *9*, 1246; i) M. Gao, W. Sheng, Z. Zhuang, Q. Fang, S. Gu, J. Jiang, Y. Yan, *J. Am. Chem. Soc.* **2014**, *136*, 7077; j) L. C. Seitz, C. F. Dickens, K. Nishio, Y. Hikita, J. Montoya, A. Doyle, C. Kirk, A. Vojvodic, H. Y. Hwang, J. K. Nørskov, T. F. Jaramillo, *Science* **2016**, *353*, 1011; k) L. Han, S. Dong, E. Wang, *Adv. Mater.* **2016**, *28*, 9266; l) M. Gong, Y. Li, H. Wang, Y. Liang, J. Z. Wu, J. Zhou, J. Wang, T. Regier, F. Wei, H. Dai, *J. Am. Chem. Soc.* **2013**, *135*, 8452; m) H. Hu, B. Guan, B. Xia, X. W. Lou, *J. Am. Chem. Soc.* **2015**, *137*, 5590; n) J. Yang, G. X. Zhu, Y. J. Liu, J. X. Xia, Z. Y. Ji, X. P. Shen, S. K. Wu, *Adv. Funct. Mater.* **2016**, *26*, 4712; o) T. Yoon, K. S. Kim, *Adv. Funct. Mater.* **2016**, *26*, 7386; p) Z. M. Luo, C. L. Tan, X. Zhang, J. Z. Chen, X. H. Cao, B. Li, Y. Zong, L. Huang, X. Huang, L. H. Wang, W. Huang, H. Zhang, *Small* **2016**, *12*, 5920.
- [6] a) Q. Gong, L. Cheng, C. Liu, M. Zhang, Q. Feng, H. Ye, M. Zeng, L. Xie, Z. Liu, Y. Li, *ACS Catal.* **2015**, *5*, 2213; b) J. Xie, J. Zhang, S. Li, F. Grote, X. Zhang, H. Zhang, R. Wang, Y. Lei, B. Pan, Y. Xie, *J. Am. Chem. Soc.* **2013**, *135*, 17881; c) M. Caban-Acevedo, M. L. Stone, J. R. Schmidt, J. G. Thomas, Q. Ding, H.-C. Chang, M.-L. Tsai, J.-H. He, S. Jin, *Nat. Mater.* **2015**, *14*, 1245.
- [7] C. C. L. McCrory, S. Jung, J. C. Peters, T. F. Jaramillo, *J. Am. Chem. Soc.* **2013**, *135*, 16977.
- [8] a) S. Dou, L. Tao, J. Huo, S. Wang, L. Dai, *Energy Environ. Sci.* **2016**, *9*, 1320; b) F. Song, K. Schenk, X. Hu, *Energy Environ. Sci.* **2016**, *9*, 473; c) X. Zhu, C. Tang, H.-F. Wang, B.-Q. Li, Q. Zhang, C. Li, C. Yang, F. Wei, *J. Mater. Chem. A* **2016**, *4*, 7245; d) X. Han, C. Yu, J. Yang, C. Zhao, H. Huang, Z. Liu, P. M. Ajayan, J. Qiu, *Adv. Mater. Interfaces* **2016**, *3*, 201500782; e) H. Kato, K. Asakura, A. Kudo, *J. Am. Chem. Soc.* **2003**, *125*, 3082; f) F. Song, X. Hu, *J. Am. Chem. Soc.* **2014**, *136*, 16481; g) X. Xu, C. Su, W. Zhou, Y. Zhu, Y. Chen, Z. Shao, *Adv. Sci.* **2016**, *3*, 1500187.
- [9] Z. Wu, L.-P. Sun, T. Xia, L.-H. Huo, H. Zhao, A. Rougier, J.-C. Grenier, *J. Power Sources* **2016**, *334*, 86.
- [10] Z. Y. Lu, L. Qian, Y. Tian, Y. P. Li, X. M. Sun, X. Duan, *Chem. Commun.* **2016**, *52*, 908.
- [11] X. Long, S. Xiao, Z. Wang, X. Zheng, S. Yang, *Chem. Commun.* **2015**, *51*, 1120.
- [12] N. Yang, C. Tang, K. Wang, G. Du, A. M. Asiri, X. Sun, *Nano Res.* **2016**, *9*, 3346.
- [13] a) J. Duan, S. Chen, A. Vasileff, S. Z. Qiao, *ACS Nano* **2016**, *10*, 8738; b) M. Risch, K. Klingan, F. Ringleb, P. Chernev, I. Zaharieva, A. Fischer, H. Dau, *ChemSusChem* **2012**, *5*, 542; c) A. Nelson, K. E. Fritz, S. Honrao, R. G. Hennig, R. D. Robinson, J. Suntivich, *J. Mater. Chem. A* **2016**, *4*, 2842.
- [14] A. Grimaud, W. T. Hong, Y. Shao-Horn, J. M. Tarascon, *Nat. Mater.* **2016**, *15*, 121.
- [15] a) Y. Ma, X. Dai, M. Liu, J. Yong, H. Qiao, A. Jin, Z. Li, X. Huang, H. Wang, X. Zhang, *ACS Appl. Mater. Interfaces* **2016**, *8*, 34396; b) B. Zhang, C. Xiao, S. Xie, J. Liang, X. Chen, Y. Tang, *Chem. Mater.* **2016**, *28*, 6934; c) X. Yu, M. Zhang, W. Yuan, G. Shi, *J. Mater. Chem. A* **2015**, *3*, 6921; d) X. Xu, F. Song, X. Hu, *Nat. Commun.* **2016**, *7*, 12324; e) J. Qi, W. Zhang, R. Xiang, K. Liu, H.-Y. Wang, M. Chen, Y. Han, R. Cao, *Adv. Sci.* **2015**, *2*, 1500199; f) L. Trotochaud, S. L. Young, J. K. Ranney, S. W. Boettcher, *J. Am. Chem. Soc.* **2014**, *136*, 6744; g) M. W. Louie, A. T. Bell, *J. Am. Chem. Soc.* **2013**, *135*, 12329; h) W. Zhang, J. Qi, K. Q. Liu, R. Cao, *Adv. Energy Mater.* **2016**, *6*, 1502489.
- [16] W. Chen, H. Wang, Y. Li, Y. Liu, J. Sun, S. Lee, J.-S. Lee, Y. Cui, *ACS Cent. Sci.* **2015**, *1*, 244.
- [17] a) X. Long, J. Li, S. Xiao, K. Yan, Z. Wang, H. Chen, S. Yang, *Angew. Chem., Int. Ed.* **2014**, *53*, 7584; b) H.-F. Wang, C. Tang, X. Zhu, Q. Zhang, *J. Mater. Chem. A* **2016**, *4*, 3379; c) B.-Q. Li, C. Tang, H.-F. Wang, X.-L. Zhu, Q. Zhang, *Sci. Adv.* **2016**, *2*, e1600495; d) G. L. Tian, Q. Zhang, B. S. Zhang, Y. G. Jin, J. Q. Huang, D. S. Su, F. Wei, *Adv. Funct. Mater.* **2014**, *24*, 5956.
- [18] C. Tang, H.-S. Wang, H.-F. Wang, Q. Zhang, G.-L. Tian, J.-Q. Nie, F. Wei, *Adv. Mater.* **2015**, *27*, 4516.
- [19] X. Long, G. Li, Z. Wang, H. Zhu, T. Zhang, S. Xiao, W. Guo, S. Yang, *J. Am. Chem. Soc.* **2015**, *137*, 11900.
- [20] Q. Liu, J. Jin, J. Zhang, *ACS Appl. Mater. Interfaces* **2013**, *5*, 5002.
- [21] B. You, Y. Sun, *Adv. Energy Mater.* **2016**, *6*, 1502333.

Received: February 22, 2017

Revised: March 17, 2017

Published online: May 16, 2017